Electrochimica Acta 213 (2016) 408–415

Contents lists available at ScienceDirect

Electrochimica Acta

journal homepage: www.elsevier.com/locate/electacta

pH dependence of quinone-mediated extracellular electron transfer in a bioelectrochemical system

Yundang Wu[a,b,c], Fangbai Li[b], Tongxu Liu[b,*], Rui Han[b], Xiaobo Luo[b]

[a] Guangzhou Institute of Geochemistry, Chinese Academy of Sciences, Guangzhou 510640, China
[b] Guangdong Key Laboratory of Agricultural Environment Pollution Integrated Control, Guangdong Institute of Eco-Environmental and Soil Sciences, Guangzhou 510640, China
[c] University of Chinese Academy of Sciences, Beijing 100049, China

ARTICLE INFO

Article history:
Received 6 April 2016
Received in revised form 19 July 2016
Accepted 21 July 2016
Available online 25 July 2016

Keywords:
pH
quinone
extracellular electron transfer
bioelectrochemical system

ABSTRACT

Quinone-mediated extracellular electron transfer (EET) is a well-known and important microbial respiration process in many natural and engineering systems. While it has been recognized that both the speciation of quinones and cell metabolism are pH-sensitive, the pH dependence of quinone-mediated EET is still unclear. In this study, pH effects in the range of 6.2 to 7.8 were investigated in a bioelectrochemical system using 9,10-anthraquinone-2-sulfonic acid (AQS) as a model quinone. The results showed that the current generation increased at pH 6.2–6.8 and then tended to stabilize, with a slight decrease at pH 7.0–7.8. The open circuit voltage (OCV) changed in a similar manner as a function of pH. The cell growth after current generation at different pH values was also indicated by the total DNA, which increased at pH 6.2–6.8 and then decreased at pH 7.0–7.8. Thermodynamic calculations and cyclic voltammetry measurements indicated that the redox potentials of AQS were negatively correlated with pH. At pH 6.2–7.0, both cell growth and the AQS redox properties had positive effects; at pH 7.0–7.8, while the AQS redox properties still had a positive impact on the EET capacity, the decline in the cell density slowed the increase of the EET capacity. These results provide a fundamental understanding of quinone-mediated EET processes and emphasize the importance of pH.

1. Introduction

Extracellular electron transfer (EET) is well-known to be a typical mechanism for microbial respiration processes with terminal electron acceptors [1–5] and has a major impact on the fate of trace metals and nutrients, as well as the degradation of organic matter [6–8]. Although direct electron transfer from bacteria to substrates via outer membrane cytochromes is considered to be the basic EET pathway, electron shuttles (ES) play a key role in facilitating long-range electron transfer from the bacterial cell surface to insoluble electron acceptors (e.g., iron(III) oxides and electrodes) via the cycling of their reduced and oxidized states [9–11]. Quinone compounds are very common types of ESs and not only widely exist in aquatic and terrestrial environments (exogenous ESs) but can also be secreted by various microorganisms (endogenous ESs) [1,12–15]. The ubiquity of quinone compounds and their particular redox properties highlight their environmental significance and their roles in EET processes [9,16]. Given that the redox behavior and the speciation of quinones varies substantially under different conditions, the mechanisms of quinone-mediated EET at the molecular level are not fully understood.

Because the cycling of reduced and oxidized quinones drives the electron shuttling processes [17], redox transformation between reduced and oxidized quinones definitely occurs. An oxidized quinone contains two carbonyls (—C=O) on the para position of a phenyl ring [18,19]. The oxidized quinone can be transformed into a semiquinone after accepting one electron and to a hydroquinone after accepting a second electron [20,21]. During this process, it has been noted that a proton (H^+) is also involved in the transformation from the quinone to the hydroquinone [20], indicating that the pH may directly affect the quinone-mediated EET process [22]. The kinetics of the hematite reduction by bio-reduced anthraquinone-2,6-disulfonate at different pH values showed a decreasing tendency of the iron reduction rate with an increase in pH from 4.5 to 7.6 [22]. The reaction system contained microbes, quinones and iron oxides, all of which might be sensitive to pH [23–25]. Based on the Nernst equation, the redox potentials

* Corresponding author.
E-mail address: txliu@soil.gd.cn (T. Liu).

http://dx.doi.org/10.1016/j.electacta.2016.07.122
0013-4686/

of the quinones and iron oxides were directly determined by their speciation as a function of pH, resulting in pH-dependent thermodynamics [26,27]. In addition, cell metabolism was also obviously affected by pH, and an optimal range of pH was favorable for cell growth [23,28] and caused a potential high efficiency of the quinone-mediated EET. However, in a complex system containing microbes, quinones and iron oxides, it was very hard to clarify which factor(s) were responsible for the changes in the iron reduction rate as a function of pH.

The study of bioelectrochemical systems (BES) is a promising approach to examine the *in situ* dynamics of EET by directly recording the microbial current generation [29,30]. The importance of the formal potential (E_h) of quinones in a quinone-mediated EET process has been highlighted in a previous study [31–35], because the E_h of quinones determined the main potential losses in a quinone-mediated EET that represented the driving force (ΔE) of the entire system [31]. Because the pH can influence the E_h of quinones, it is likely to further change ΔE as well as the overall electron transport efficiency in the BES. In addition, the optimal pH may be very favorable for cell growth of biofilm on the electrodes [36], resulting in further influencing the EET capacity in the BES. Hence, pH changes may both induce the alternation of quinone speciation and cell growth and, eventually, the rate and extent of quinone-mediated EET processes.

In this study, 9,10-anthraquinone-2-sulfonic acid (AQS), which can be easily measured by UV/Visible spectroscopy [31], was used as a model quinone in a BES with the classical strain *Shewanella oneidensis* MR-1[23]. Current generation and open circuit voltages were examined at different pH values. The electrochemical measurements, the speciation of AQS, and the cell growth were integrated in this study (i) to examine the effects of pH on the capacity of a quinone-mediated EET and (ii) to reveal possible factors responsible for pH-dependent effects in the presence of AQS. These observations may help us improve our fundamental understanding of the mechanisms involved in a quinone-mediated EET under various environmental conditions.

2. Experimental

2.1. Cell growth and materials

Shewanella oneidensis MR-1 (MR-1) was isolated from anoxic sediments from Lake Oneida, NY [23], and purchased from MCCC (Marine Culture Collection of China, China). The strain was cultured aerobically at 30 °C and shaken continuously at 180 rpm in LB medium until the mid-exponential phase was reached. Cell growth was determined by measuring the optical density at 600 nm (OD600). The cell suspension was centrifuged, washed and diluted to the desired concentration for subsequent bioelectrochemical experiments. The 9,10-anthraquinone-2-sulfonic acid (AQS, AR, 98.0%) was obtained from Acros (China). Other chemicals were purchased from Guangzhou Chemical Reagent Factory (Guangzhou, China). in China. All solutions were prepared using Milli-Q deoxygenated ultrapure water (18 MΩ cm, Easy Pure'II RF/UV, USA).

2.2. The BES setup and electrochemical measurements

A potentiostat (CHI660D, Chenhua Co., Ltd., Shanghai, China) was used for electrochemical measurements. A MR-1 (2×10^8 cells mL^{-1}) suspension (110 mL) was cultivated in the presence of 50 mM lactate and 50 μM AQS in a serum bottle under anoxic conditions. The BES was equipped with three electrodes on the top of the serum bottle that held the MR-1 suspension (Fig. 1a). Two pieces of carbon cloth (2 cm × 6 cm) were used as a working electrode and a counter electrode. A calomel electrode was used as a reference electrode. A fixed-potential of 0.441 V (vs. SHE) was applied to the BES and controlled by the potentiostat. As a comparison, the current generation experiment was also carried out on flat glassy carbon electrode instead of carbon felt electrode. The device was shown in Fig. S1a. A flat glassy carbon (10 × 10 mm) was used as a working electrode in order to provide a smooth surface and reduce the biofilm formation. The BES was subjected to three phases (Phase I, open circuit; Phase II, closed circuit; Phase III, open circuit). During Phase I and Phase III, the open circuit voltage (OCV) was recorded for 2 hours to obtain a steady-state OCV value. During Phase II, the current generation was measured for 48 h. Low scan rate cyclic voltammetry (CV) (1 mV s^{-1}) in Phase III was performed after 2 days of current generation. The CV of the AQS solution was measured at different pH values after purging with oxygen-free N_2 for 10 min at a 50 mV s^{-1} scan rate, and a glassy carbon electrode, a palladium wire electrode, and a calomel electrode were used as the working electrode, counter electrode, and reference electrode, respectively. The solution/suspension pH in the range of 6.2 to 7.8 was adjusted with 200 mM phosphate buffer (PBS). Solutions containing NH_4Cl (1.24 g L^{-1}), KCl (0.52 g L^{-1}), a vitamin stock solution (5 mg L^{-1}), and a mineral stock solution (12.5 mg L^{-1}) [37] were also added to the cell suspension to maintain cell growth.

2.3. Spectroelectrochemical measurements

The speciation of AQS varied during the potentiostatic incubation of MR-1 in the presence of AQS and could be directly measured by UV-Visible absorption spectroscopy. In addition, the outer membrane *c*-Cyts could also be measured by UV-Visible diffuse-transmittance absorption spectroscopy. To monitor the spectra of the AQS and the outer membrane *c*-Cyts in the BES, a wide quartz cuvette (1 cm path, 5 cm width) equipped with three electrodes (Fig. 1b) was used to simultaneously measure the electricity and spectra of AQS and the outer membrane *c*-Cyts in the cell suspension via diffuse-transmittance absorption spectroscopy (TU-

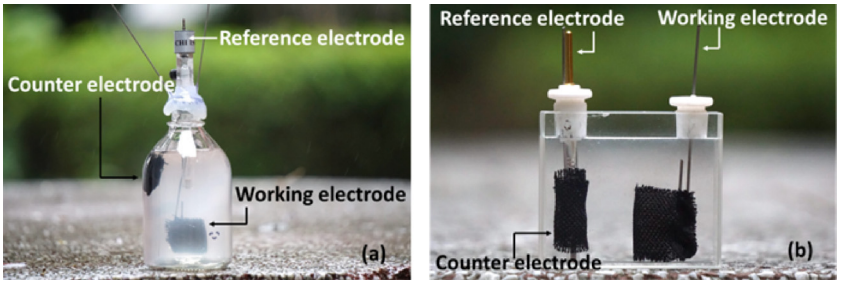

Fig. 1. (a) A depiction of a bioelectrochemical system. Working electrode and counter electrode: carbon cloth; reference electrode: calomel electrode. (b) An image of a spectroelectrochemical system, which is a custom-made anaerobic quartz cuvette. Working electrode and counter electrode: carbon cloth; reference electrode: Ag/AgCl electrode.

1901 Beijing, China) combined with an electrochemical workstation (CHI660D, Chenhua Co. Ltd., Shanghai, China).

2.4. Microbiology measurements

Because bacteria adhered to the carbon cloth electrodes, a Power Soil® DNA isolation kit from Mobio Laboratories, Inc. (USA), was used to extract DNA from the carbon electrode following the manufacturer's instructions. A DNA solution (100 μL) was obtained. The DNA concentration (10 μL) was measured with an Invitrogen Qubit® 2.0 Fluorometer (Thermo Fisher, USA) using a fluorescent reagent and calibrated using the standard sample provided by the manufacturer. DNA extraction for the experiments was conducted in triplicate, and the mean values and error bars were derived from the average and standard deviation values calculated from three replicates. The morphology of cells on the carbon cloth electrodes were examined by with a scanning electron microscope (SEM, S-3000N, Hitachi). The samples were soaked in a 2.5% glutaraldehyde solution for 5 hours to keep intact without any damage to the cells and then dehydrated in an ethanol gradient and t-BuOH. Finally, the sample was coated with evaporated platinum before being viewed via SEM with an operating voltage of 15 kV.

3. Results

3.1. Electricity generation by MR-1 with AQS at different pH values

The current density and OCV in BES with MR-1 and AQS were investigated at pH 6.2–7.8. While no current was generated in Phase I and Phase III due to the open circuit conditions, the results revealed that the current in Phase II in the BES with AQS increased gradually at the beginning (0–20 h) and then the output became constant after approximately 20 h, as shown in Fig. 2a. The maximum constant current (I_{max}) showed that the I_{max} value at pH 6.2 was only 0.76 A m^{-2}, but when the pH was increased to 6.8, the I_{max} value was substantially increased to ~2.1 A m^{-2} and then slightly decreased to ~1.9 A m^{-2} as the pH increased to 7.8, as shown in Fig. 2b. The maximum current generation was observed at pH 6.8. The OCV values in Phase I (OCV_I) and Phase III (OCV_{III}) as a function of pH are plotted in Figs. 2c and 2d. The results show that the OCV_I decreased in a step-wise manner from pH 6.2 to 7.8, while the OCV_{III} decreased from pH 6.2 to 6.8 and then slightly increased at pH values from 7 to 7.8. In addition, the OCV_{III} was more negative than the OCV_I at the same pH. While a high correlation coefficient (R^2) of 0.89 was observed between OCV_I and pH, weak correlation was observed for I_{max} vs pH (R^2 = 0.48), and OCV_{III} vs pH (R^2 = 0.19), respectively.

Because *Shewanella* has the capacity of producing riboflavin which will eventually increase EET rate, the role of the endogenous flavins on EET rates was examined. Firstly, the supernatant was collected from the MR-1 suspension cultured without any electron mediator in the BES. Results in Fig. S2a showed that the peaks at 372 and 445 nm were attributed to 2 μM riboflavin, but no obvious peak observed in the supernatant of suspension, suggesting that the absorbance of self-secreted riboflavin in the BES was much lower than 2 μM riboflavin, and far less than AQS (50 μM) used in this study. Hence, the effect of self-secreted riboflavin on the EET rates in the bioelectrochemical system may be neglected due to its tiny amount. Secondly, the current generations at pH 7 with exogenous riboflavin (2 μM), AQS (50 μM) and without exogenous electron mediator were examined in the BES. Results in Fig. S2b showed that the maximum current in the treatment with 2 μM exogenous riboflavin was 17-times higher than the treatment without exogenous electron mediator, and the current in the treatment with 50 μM AQS was even 38-times higher than the treatment without exogenous electron mediator. This suggested that the influence of self-secreted riboflavin on the current generation can be ignored.

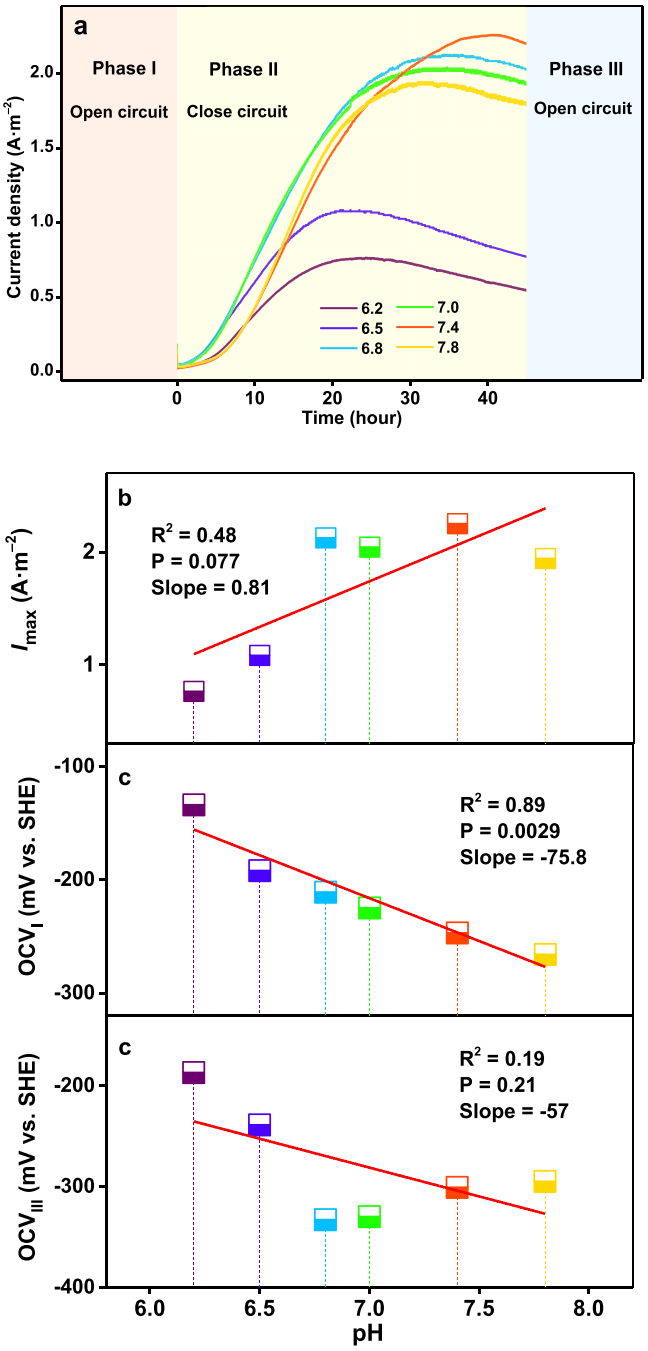

Fig. 2. (a) Current density vs. time at different pH values (6.2–7.8). The anaerobic potentiostatic cultivation of MR-1 (2×10^8 cells ml^{-1}) was performed with 50 mM lactate and 50 μM AQS at a fixed-potential of 0.441 V (vs. SHE); (b) The I_{max} of Phase II as a function of pH. (b) The open circuit voltage was measured in Phase I and Phase III as a function of pH.

3.2. CVs of BES with MR-1 and AQS under different pH

Because it was demonstrated that slow scan-rate voltammetry can detect electron transfer between bacteria and electrodes [38], the CVs of all of the BES in Phase III at pH 6.2–7.8 were conducted with a slow scan rate (1 mV s^{-1}). The results in Fig. 3a reveal a

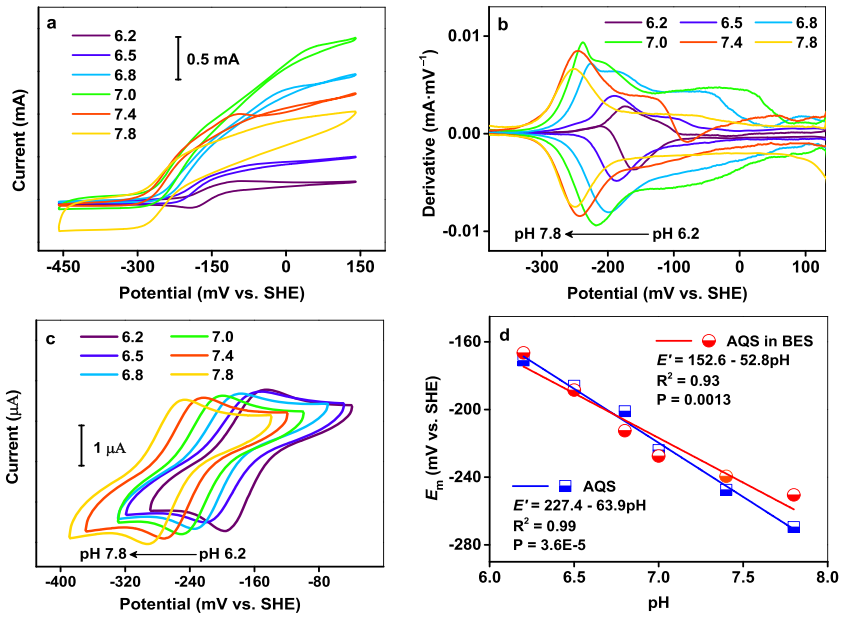

Fig. 3. (a) The CVs of BES with AQS at different pH obtained from a slow-rate scan (1 mV s^{-1}). The measurement was performed in the bioelectrochemical system after a potentiostatic incubation. (b) The first derivative analysis of the CV results; (c) Cyclic voltammograms of AQS at different pH value, obtained using a glassy carbon electrode as the working electrode after 10 min of oxygen-free N_2 purging. (d) Linear correlation between midpoint potential of AQS (E_m) and pH.

sigmoidal anodic current profile characteristic of catalytic activity, which was a typical biofilm shape [38]. The CV maximum catalytic current increased from pH 6.2–6.8 and then slightly decreased from pH 7 to 7.8. A first derivative analysis of the voltammetry results allowed the estimation of the potential at which the rate of increase of the catalytic wave reached a maximum [39]. To distinguish the redox peaks of the biofilm and AQS, the first derivative analysis of CVs showed that two strong symmetrical peaks were observed on the left side of each curve in all treatments and that the peak position shifted negatively as the pH increased from 6.2 to 7.8, as shown in Fig. 3b, which could be attributed to the redox cycling of the AQS. Additionally, the weak peaks on the shoulder could also be attributed to redox proteins [40]. The CVs of pure AQS at different pH values were examined. The results shown in Fig. 3c demonstrate that symmetrical voltammetry results were observed for AQS at different pH values, revealing that the redox transformation of AQS was fully reversible. Both the midpoint potentials (E_m) of AQS in BES and pure AQS are plotted as a function of pH in Fig. 3d, which shows a linear relationship with a very similar slope of 52.8 for AQS in BES and 63.9 for pure AQS.

3.3. Spectra of AQS and MR-1 in the BES under different pH

The results shown in Fig. 4a demonstrate the absorption spectra of the BES with MR-1 and AQS. The spectrum of MR-1 in the absence of AQS showed a typical pattern of reduced *c*-Cyts, with characteristic peaks at 419 nm and 552 nm. The peak at 330 nm was attributed to oxidized AQS (AQS_{ox}) as indicated by the spectrum of pure AQS_{ox} in Fig. 4b. Upon incubation with MR-1 in Phase I, the partial AQS_{ox} was transformed into a reduced form (AQS_{red}) with a characteristic peak at 383 nm, as indicated by the spectrum of AH_2QS. It was noted that the peak at 383 nm decreased gradually as the pH increased from 6.2 to 7.8. After current was generated (Phase III), more AQS_{ox} was transformed into AQS_{red} (AH_2QS and AHQS) and the peak at 330 nm decreased and that at 383 nm increased. A very small peak was also evident at 400 nm, as indicated by the spectrum of AHQS at pH 7.4 and 7.8.

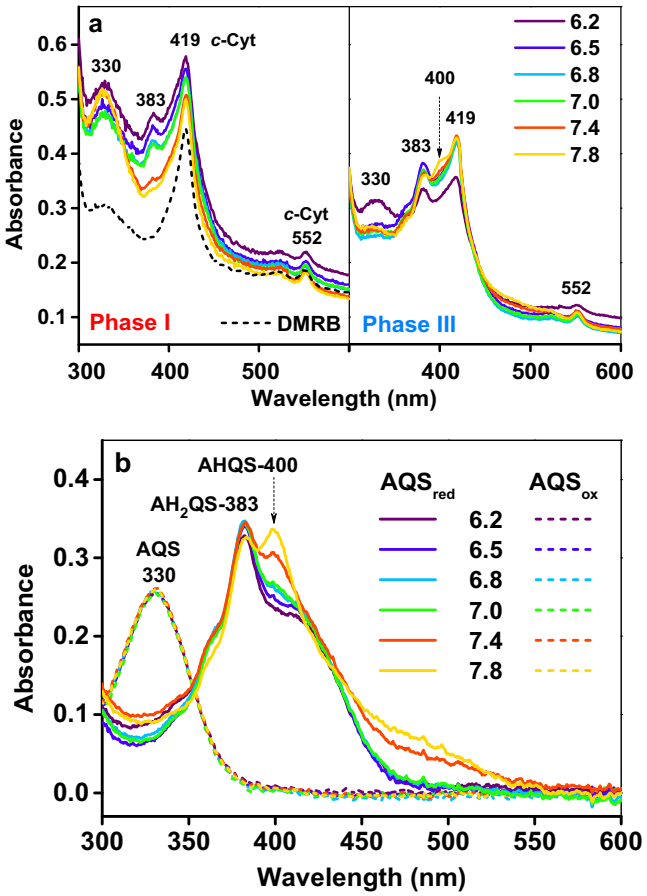

Fig. 4. (a) UV/Vis diffuse-transmittance absorption spectra of the spectroelectrochemical system obtained in Phase I and Phase III. The potentiostatic measurement was performed in the presence of 50 mM lactate and 50 μM AQS under a fixed-potential of 0.441 V (vs. SHE) (b) The spectra of oxidized AQS (AQS_{ox}) and reduced AQS (AQS_{red}) was obtained via an electrochemical reduction.

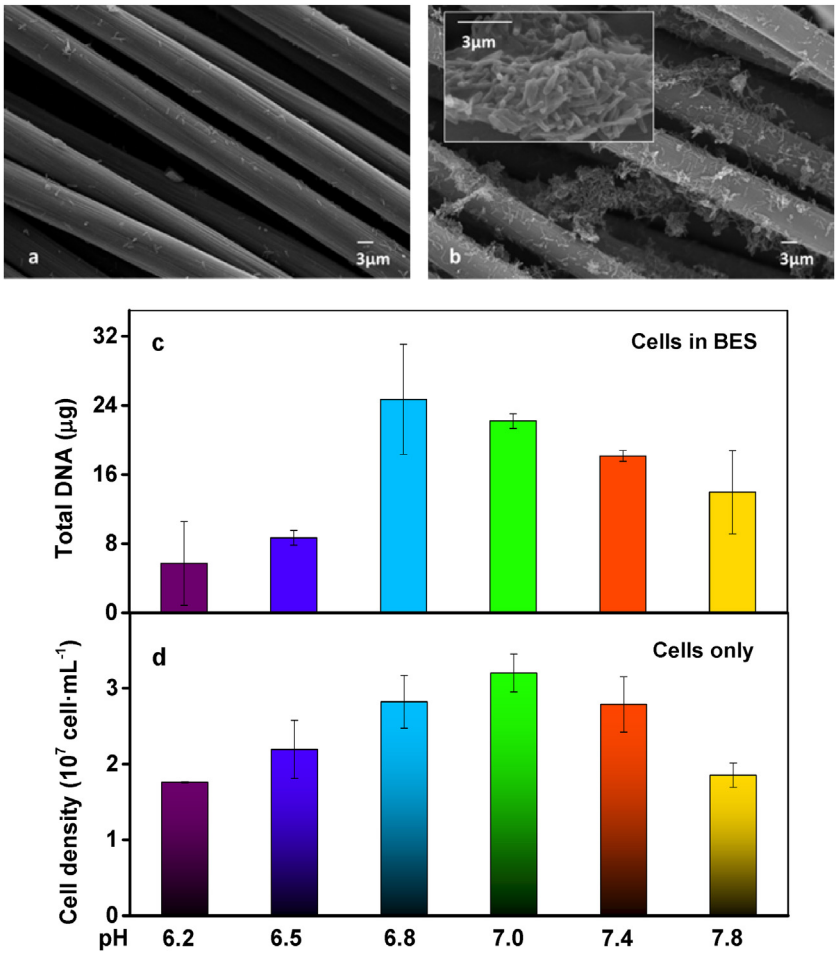

Fig. 5. SEM images of the electrodes at pH 7 in Phase I (a) and Phase III (b). The total bacteria DNA in Phase III of BES at different pH (c) and the cell density of the cells only incubated in anaerobic cuvettes with AQS (3.3 mM) as electron acceptors (d).

3.4. Cell growth under different pH

SEM images of the carbon cloth electrode before and after potentiostatic incubation at pH 7 are shown in Figs. 5a and 5b, which obviously shows that a biofilm was observed in Phase III after 2 days of current generation. To quantitatively illustrate the dynamics of the biofilm formation and cell growth, the total DNA of the biofilm on the carbon cloth electrode under different pHs was extracted and measured. The results in Fig. 5c show that the total DNA increased from pH 6.2 to 6.8 and then slightly decreased from pH 7 to 7.8. In comparison, the cell growth with AQS (3.3 mM) in an anaerobic cuvette under anoxic conditions was examined. The results in Fig. 5d show that the cell density increased from pH 6.2 to 7.0 and then decreased from pH 7 to 7.8.

4. Discussion

4.1. The reactions of AQS-mediated EET processes

It has been well-documented that *c*-Cyts in the outer membrane were involved in the electron transfer processes during the current generation by MR-1 [41,42]. Specifically, the electron transfer pathway in an anode chamber with MR-1 and AQS includes intracellular electron transport (IET), extracellular electron transfer (EET), and the diffusion of reduced AQS to the anode electrode. The step-wise potential losses can drive the electron flow from the electron donor to the anode, resulting in the generation of a current. In the IET process, the following half-cell reaction (Rxn. 1) determines the electron production rates and the concomitant anode potential:

$$C_3H_5O_3^- + 2H_2O \rightarrow C_2H_3O_2^- + HCO_3^- + 5H^+ + 4e^- \quad \text{(Rxn.1)}$$

Hence, according to the Nernst equation, the specific theoretical redox potential of the electron donor can be derived by Eq. (1).

$$E_{C_3H_5O_3^-} = E^0_{C_3H_5O_3^-} - 0.015\ln\frac{[C_2H_3O_2^-][HCO_3^-]}{[C_3H_5O_3^-]} + 0.17\text{pH} \quad (1)$$

Apparently, the redox potential of lactate increases with increasing pH, indicating that the reducing ability of electron donor decreases as the pH increases. In addition, the pH in Phase III dropped by 0.2–0.3 units compared with the pH in Phase I, which could further confirm the proton release that occurs in Rxn. 1.

As a result of the IET processes, *c*-Cyt_{ox} was reduced to *c*-Cyt_{red}, followed by the occurrence of EET processes via electron transfer from *c*-Cyt_{red} to AQS (Rxn. 2).

$$c\text{–}Cyt_{red} + AQS_{ox} \leftrightarrow c\text{–}Cyt_{ox} + AQS_{red} \quad \text{(Rxn.2)}$$

The half reaction for *c*-Cyts transformation is shown in Rxn. 3:

$$c\text{–}Cyt_{ox} + 2e^- \leftrightarrow c\text{–}Cyt_{red} \quad \text{(Rxn.3)}$$

The redox potentials of the *c*-Cyts ($E_{c\text{-}Cyt}$) can be calculated from Eq. (2):

$$E_{c-Cyt} = E^0_{c-Cyt} - \frac{RT}{nF}\ln\frac{[c-Cyt_{red}]}{[c-Cyt_{ox}]} \quad (2)$$

The half reaction for AQS transformation is shown in Rxn. 4:

$$AQS + 2H^+ + 2e^- \leftrightarrow AH_2QS \quad \text{(Rxn.4)}$$

The redox potentials of AQS (E_{AQS}) can be calculated from Eq. (3):

$$E_{AQS} = E^0_{AQS} - 0.0295\ln\frac{[AH_2QS]}{[AQS]} - 0.059pH \quad (3)$$

The standard redox potential at a specific pH can be calculated from Eq. (4).

$$E_{AQS}' = E^0_{AQS} - 0.059pH \quad (4)$$

The driving force of the IET process and the AQS-mediated EET process are indicated by Eqs. (5) and (6).

$$\Delta E_{IET} = E_{C_3H_5O_3^-} - E_{c-Cyt} \quad (5)$$

$$\Delta E_{EET} = E_{c-Cyt} - E_{AQS} \quad (6)$$

Hence, both ΔE_{IET} and ΔE_{EET} were directly affected by the pH due to the involvement of H^+ in the reactions. The pH changes may affect the proton release in Rxn. 1 and ultimately affect $E_{C_3H_5O_3^-}$ and ΔE_{IET}. The pH changes may also affect the proton consumption in Rxn. 4 and ultimately affect $E_{c\text{-}Cyt}$ and ΔE_{EET}.

In the diffusion process, AQS_{red} diffused to the anode surface and concomitantly transferred electrons from AQS_{red} to the anode, resulting in the generation of current (Rxn. 5):

$$AQS_{red} + Anode \rightarrow Anode \cdot AQS_{red} \rightarrow AQS_{ox} + Current \quad \text{(Rxn.5)}$$

The transport of soluble AQS_{red} to the anode is a slow diffusion process governed by Fick's law [43], and the diffusion process can be calculated by Eq. (7).

$$j = nF\left(\frac{D_{AQS}\Delta[AQS_{red}]}{\Delta z}\right) \quad (7)$$

where j is the current density ($A\,m^{-2}$), D_{AQS} is the diffusion coefficient of the AQS ($m^2\,s^{-1}$), Δz is the transport distance (m), $\Delta[AQS_{red}]$ is the concentration gradient of AQS_{red} ($mol\,m^{-3}$), and nF is a conversion factor from moles to coulombs. It can be speculated that the diffusion process is not pH-dependent because H^+ is not involved.

4.2. Roles of pH-dependent AQS redox properties

The aforementioned results indicate that the AQS-mediated EET at different pH values was affected by the AQS redox properties, such as the redox speciation and redox potential of AQS. To examine the role of the AQS redox properties on AQS-mediated electricity generation, a linear regression of I_{max}, OCV_I and OCV_{III} was plotted as a function of the standard redox potential of AQS at a specific pH, which was indicated by the midpoint redox potential (E_m). The results in Fig. 6a show that a high correlation coefficient (R^2) of 0.86 was obtained between E_m and OCV_I, indicating that the initial OCV of the system was dominated by the redox properties of AQS. However, the results shown in Fig. 6b demonstrate that a weak correlation was observed between OCV_{III} and E_m ($R^2 = 0.21$). Similar to OCV_{III}, the results shown in Fig. 6c also demonstrate a weak correlation between I_{max} and E_m ($R^2 = 0.45$).

The slope of E_m versus pH was 52.8 mV, which is close to the theoretical value 59 mV based on Eq. (4), revealing that the AQS-mediated EET process was a proton-coupled electron transfer reaction. A spectral analysis of the cell suspension with AQS (Fig. 4a) indicated that AH_2QS was the single reduced form of AQS at all pH values at the beginning of Phase II, but the peak of AH_2QS

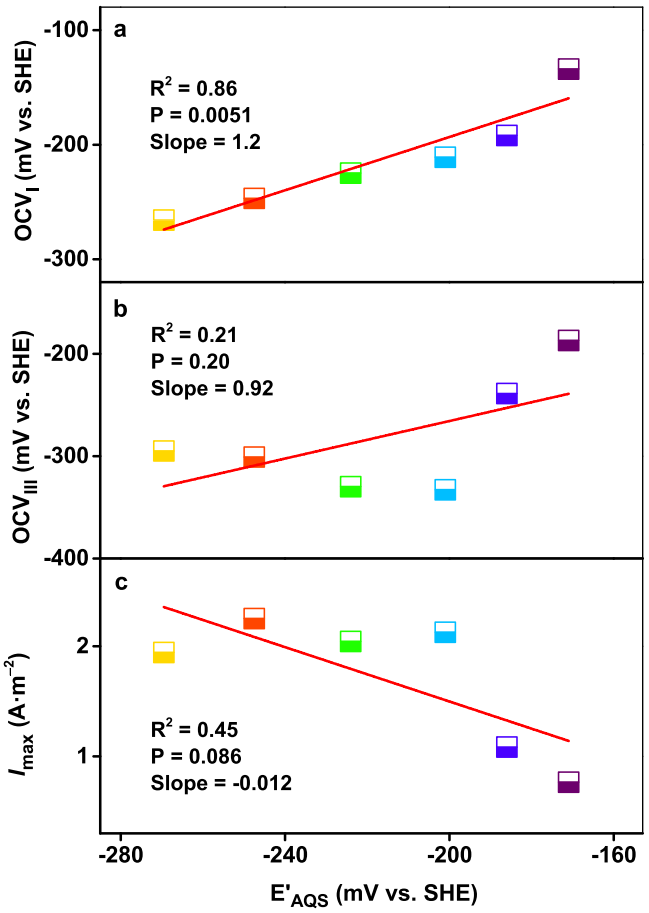

Fig. 6. (a) Linear correlation between OCV_I and standard potential of AQS (E_m). (b) Linear correlation between OCV_{III} and standard potential of AQS (E_m). (c) Linear correlation between I_{max} and standard potential of AQS (E_m).

at 383 nm gradually decreased with increasing pH because the E_m became more negative at a high pH according to Fig. 3c (CV of AQS), making it difficult for OM *c*-Cyt_{red} to reduce the AQS_{ox}. At the end of Phase II, a small peak at 400 nm for AHQS appeared at pH 7.8. The following half reactions were supposed to occur (Rxns. 6 and 7). Only one electron is needed for AHQS generation, while two electrons are needed for AH_2QS generation, suggesting the electron-carrier capacity at pH 7.8 may be lower than that at pH <7.8, which may be responsible for the lower I_{max} and OCV_{III} at pH 7.8.

$$AQS + H^+ + e^- \leftrightarrow AHQS \quad \text{(Rxn.6)}$$

$$AHQS + H^+ + e^- \leftrightarrow AH_2QS \quad \text{(Rxn.7)}$$

Therefore, the effects of pH on the AQS-mediated EET were attributed to the different AQS speciation and the involvement of protons in the reactions.

4.3. Role of pH-dependent cell growth

It was well-documented that cell growth was also obviously affected by pH [23,28] and might cause the changes in the quinone-mediated EET. To examine the role of cell growth as indicated by total DNA on AQS-mediated electricity generation, a linear regression of I_{max} and OCV_{III} as a function of DNA was plotted in Fig. 7. The results shown in Figs. 7a and b demonstrate that a linear relationship was observed for I_{max} and OCV_{III} as a function of DNA

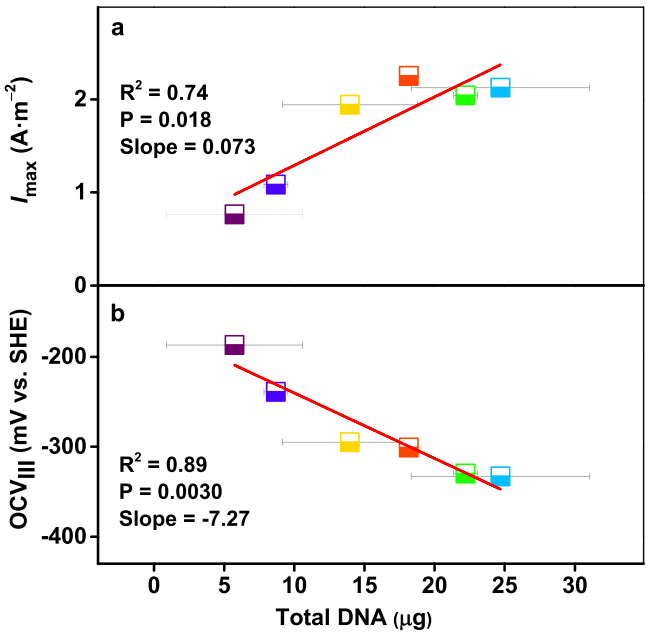

Fig. 7. (a) Linear correlation between I_{max} and total DNA. (b) Linear correlation between OCV_{III} and total DNA.

with a correlation coefficient (R^2) of 0.74 and 0.89, respectively, implying that cell growth was also an essential factor affecting the AQS-mediated EET. The results of cell growth in the anaerobic cuvettes showed that the optimal pH of MR-1 was 7.0, indicating that the fastest rates of cell growth occurred at pH 7 [44], so it is not surprising that a high cell density leads to a high lactate consumption rate and a high electron output via IET and EET, resulting in the linear correlation between OCV_{III} and total DNA. In addition, it was noted that the R^2 value of OCV_{III} vs. total DNA (0.89) was much higher than that of OCV_{III} vs. E_m (0.21), suggesting that the contribution of pH-dependent cell growth was much greater than the contribution of pH-dependent AQS redox properties to the overall quinone-mediated EET capacity.

From the cell density and current generation at pH from 7 to 7.8 in Fig. 5c, the current generation did not decreased significantly due to the substantial decay of cell density, implying that the more negative redox potentials of AQS at pH 7–7.8 may play an important role of maintaining the current generation at a high level. To further evaluate the roles of pH-dependent AQS redox properties to EET capacity, the current generation experiment was carried out on flat glassy carbon electrode instead of carbon felt electrode in order to provide a smooth surface and reduce the biofilm formation. Results in Fig. S1b showed the current generation with flat glassy carbon electrode ($<50\,mA\,m^{-2}$) was much lower than that with carbon felt electrode ($<2.5\,A\,m^{-2}$). Results in Fig. S1c showed that the current generation increased from pH 6.2 to 7.4 and then decreased from pH 7.4 to 7.8. While the optimal pH for cell growth was at pH 7.0, the current generation kept increasing at pH from 7.0 to 7.4, suggesting that the pH-related changes of AQS redox potential might play an important role in maintaining the current generations at a high level. The current decreased from 7.4 to 7.8 eventually, highlighting the importance of pH on cell growth in the EET process. Therefore, both of cell growth and AQS redox potentials played important roles in pH-dependent EET processes.

Based on the aforementioned discussion on the role of AQS redox properties and cell growth at different pH values, the pH-dependence of both the AQS redox properties and cell growth contribute to the quinone-mediated EET processes. When the pH in BES is below the optimal pH of 7 for MR-1 cell growth, both cell growth and the AQS redox properties have positive effects on the increase in the EET capacity. When the pH is higher than the optimal pH of 7, while the AQS redox properties still have a positive impact on the EET capacity, a decline in the cell density slows the increase in the EET capacity.

5. Conclusion

In this study, the effects of pH values from 6.2 to 7.8 were investigated in a bioelectrochemical system using 9,10-anthraquinone-2-sulfonic acid (AQS) as a model quinone. The results showed that the current generation increased from pH 6.2 to 6.8 and then decreased slightly from pH 7.0 to 7.8. The open circuit voltage (OCV) changed as a function of pH in a similar manner. Cell growth after incubation under different pH conditions was also indicated by the total DNA concentration, which also increased from pH 6.2 to 6.8 and then decreased from pH 7.0 to 7.8. Thermodynamic calculations and cyclic voltammetry measurements indicated that the AQS redox potential was negatively correlated with pH. From pH 6.2 to 7.0, both cell growth and the AQS redox properties have positive effects; from pH 7.0 to 7.8, while the AQS redox properties still have a positive impact on the EET capacity, a decline in the cell density slows the increase in the EET capacity. These results provide a fundamental understanding of the quinone-mediated EET processes and highlight the importance of pH.

Acknowledgements

This work was funded by the National Natural Science Foundations of China (41522105 and 41571130052), the Guangdong Natural Science Funds for Distinguished Young Scholars (2014A030306041) and Special Support Program(2016).

Appendix A. Supplementary data

Supplementary data associated with this article can be found, in the online version, at http://dx.doi.org/10.1016/j.electacta.2016.07.122.

References

[1] E. Marsili, D.B. Baron, I.D. Shikhare, D. Coursolle, J.A. Gralnick, D.R. Bond, Proc. Natl. Acad. Sci. U.S.A. 105 (2008) 3968.
[2] G.F. White, Z. Shi, L. Shi, Z. Wang, A.C. Dohnalkova, M.J. Marshall, J.K. Fredrickson, J.M. Zachara, J.N. Butt, D.J. Richardson, Proc. Natl. Acad. Sci. U.S.A. 110 (2013) 6346.
[3] Y.A. Gorby, S. Yanina, J.S. McLean, K.M. Rosso, D. Moyles, A. Dohnalkova, T.J. Beveridge, I.S. Chang, B.H. Kim, K.S. Kim, Proc. Natl. Acad. Sci. U.S.A. 103 (2006) 11358.
[4] M.Y. El-Naggar, G. Wanger, K.M. Leung, T.D. Yuzvinsky, G. Southam, J. Yang, W. M. Lau, K.H. Nealson, Y.A. Gorby, Proc. Natl. Acad. Sci. U.S.A. 107 (2010) 18127.
[5] X. Li, T. Liu, K. Wang, T.D. Waite, Environ. Sci. Technol. 49 (2015) 1392.
[6] T. Borch, R. Kretzschmar, A. Kappler, P.V. Cappellen, M. Ginder-Vogel, A. Voegelin, K. Campbell, Environ. Sci. Technol. 44 (2009) 15.
[7] D. Lovley, Dissimilatory Fe (III)-and Mn (IV)-reducing prokaryotes, The prokaryotes, Springer, 2006, pp. 635.
[8] F. Cao, T.X. Liu, C.Y. Wu, F.B. Li, X.M. Li, H.Y. Yu, H. Tong, M.J. Chen, J. Agric. Food Chem. 60 (2012) 11238.
[9] K. Watanabe, M. Manefield, M. Lee, A. Kouzuma, Curr. Opin. Biotechnol. 20 (2009) 633.
[10] S.J. Fuller, D.G. McMillan, M.B. Renz, M. Schmidt, I.T. Burke, D.I. Stewart, Appl. Environ. Microbiol. 80 (2014) 128.
[11] H. Zhang, E.J. Weber, Environ. Sci. Technol. 43 (2009) 1042.
[12] D.R. Lovley, J.D. Coates, E.L. Blunt-Harris, E.J. Phillips, J.C. Woodward, Nature 382 (1996) 445.
[13] D.K. Newman, R. Kolter, Nature 405 (2000) 94.
[14] N. Ratasuk, M.A. Nanny, Environ. Sci. Technol. 41 (2007) 7844.
[15] E.D. Brutinel, J.A. Gralnick, Appl. Microbiol. Biotechnol. 93 (2012) 41.
[16] I. Bauer, A. Kappler, Environ. Sci. Technol. 43 (2009) 4902.
[17] A. Okamoto, K. Hashimoto, K.H. Nealson, Angewandte Chemie International Edition 53 (2014) 10988.

[18] M. Hernandez, D. Newman, Cellular and Molecular Life Sciences CMLS 58 (2001) 1562.
[19] M.E. Hernandez, A. Kappler, D.K. Newman, Appl. Environ. Microbiol. 70 (2004) 921.
[20] Z. Shi, J.M. Zachara, L. Shi, Z. Wang, D.A. Moore, D.W. Kennedy, J.K. Fredrickson, Environ. Sci. Technol. 46 (2012) 11644.
[21] A. Okamoto, K. Hashimoto, K.H. Nealson, R. Nakamura, Proc. Natl. Acad. Sci. U.S. A. 110 (2013) 7856.
[22] C. Liu, J.M. Zachara, N.S. Foster, J. Strickland, Environ. Sci. Technol. 41 (2007) 7730.
[23] C.R. Myers, K.H. Nealson, Science 240 (1988).
[24] C.I. Torres, A. Kato Marcus, B.E. Rittmann, Biotechnol. Bioeng. 100 (2008) 872.
[25] S. Orsetti, C. Laskov, S.B. Haderlein, Environ. Sci. Technol. 47 (2013) 14161.
[26] M. Uchimiya, A.T. Stone, Geochim. Cosmochim. Acta 70 (2006) 1388.
[27] J.T. Babauta, H.D. Nguyen, H. Beyenal, Environ. Sci. Technol. 45 (2011) 6654.
[28] M. Koussémon, Y. Combet-Blanc, B. Ollivier, Curr. Microbiol. 46 (2003) 0141.
[29] G.D. Schrott, P.S. Bonanni, L. Robuschi, A. Esteve-Nuñez, J.P. Busalmen, Electrochim. Acta 56 (2011) 10791.
[30] A. Okamoto, R. Nakamura, K. Hashimoto, Electrochim. Acta 56 (2011) 5526.
[31] Y. Wu, T. Liu, X. Li, F. Li, Environ. Sci. Technol. 48 (2014) 9306.
[32] E.J. O'Loughlin, Environ. Sci. Technol. 42 (2008) 6876.
[33] M. Wolf, A. Kappler, J. Jiang, R.U. Meckenstock, Environ. Sci. Technol. 43 (2009) 5679.
[34] X. Li, T. Liu, L. Liu, F. Li, RSC Advances 4 (2014) 2284.
[35] X. Li, L. Liu, T. Liu, T. Yuan, W. Zhang, F. Li, S. Zhou, Y. Li, Chemosphere (2013).
[36] T. Romeo, Bacterial Biofilms Current Topics, Microbiology and Immunology, Springer, 2008.
[37] X. Li, S. Zhou, F. Li, C. Wu, L. Zhuang, W. Xu, L. Liu, J. Appl. Microbiol. 106 (2009) 130.
[38] S. Srikanth, E. Marsili, M.C. Flickinger, D.R. Bond, Biotechnol. Bioeng. 99 (2007) 1065.
[39] F.A. Armstrong, Curr. Opin. Chem. Biol. 9 (2005) 110.
[40] E. Marsili, J.B. Rollefson, D.B. Baron, R.M. Hozalski, D.R. Bond, Appl. Environ. Microbiol. 74 (2008) 7329.
[41] D. Coursolle, J.A. Gralnick, Mol. Microbiol. 77 (2010) 995.
[42] L. Shi, D.J. Richardson, Z. Wang, S.N. Kerisit, K.M. Rosso, J.M. Zachara, J.K. Fredrickson, Environmental Microbiology Reports 1 (2009) 220.
[43] C.I. Torres, A.K. Marcus, H.S. Lee, P. Parameswaran, R. Krajmalnik-Brown, B.E. Rittmann, FEMS Microbiol. Rev. 34 (2009) 3.
[44] L. Philip, L. Iyengar, C. Venkobachar, Journal of Environmental Engineering 124 (1998) 1165–1170.